**ORIGINAL PAPER**

CrossMark

# Study on electrochemical performance of Mg-doped Li$_2$FeSiO$_4$ cathode material for Li-ion batteries

Ling Li[1] · Enshan Han[1] · Pengjun Yang[1] · Lingzhi Zhu[1] · Yuansheng Liu[1]

**Abstract**

In this paper, Li$_2$Fe$_{1-y}$Mg$_y$SiO$_4$/C ($y$ = 0, 0.01, 0.02, 0.03, 0.05), a cathode material for lithium-ion battery was synthesized by solid-state method and modified by doping Mg$^{2+}$ on the iron site. The effects of Mg$^{2+}$ doping on the crystal structure and electrochemical performance Li$_2$FeSiO$_4$ was investigated by X-ray diffraction (XRD), scanning electron microscopy (SEM), and electrochemical tests. Electrochemical methods of measurement were applied including constant current charge–discharge test, cyclic voltammetry (CV), and electrochemical impedance spectroscopy (EIS), to determine the electrochemical performance of the material and the optimal doping ion and ratio. The results showed that Li$_2$Fe$_{0.98}$Mg$_{0.02}$SiO$_4$/C has the higher specific capacity and better cycle stability as well as lower impedance and better reversibility. The enhanced electrochemical performance can be attributed to the increased electronic conductivity, the decreased charge transfer impedance, and the improved Li-ion diffusion coefficient. Then, further study on the synthesis conditions was performed to find the optimal combustion temperature and time. According to the study, the material which has the best electrochemical performance, shows initial discharge specific capacity of 142.3 mAh g$^{-1}$ at 0.1 C (1 C = 166 mA g$^{-1}$) and coulomb efficiency of 95.6%, under the condition that the temperature is 700 °C and the calcining time is 10 h.

**Keywords** Li$_2$FeSiO$_4$ · Solid-state method · Mg$^{2+}$doping · Li-ion battery · Electrochemical performance

## Introduction

In recent years, silicate polyanion material of lithium electrodes Li$_2$MSiO$_4$ (M = Mn$^{2+}$, Co$^{2+}$, Fe$^{2+}$) has been paid widely attention to [1–13]. The structure of this material is quite steady, because the Si-O bonds are very strong. Besides, the Si-O bond is shorter because the Si radius is shorter than that of the P, so the ionic conductivity of Li$_2$MSiO$_4$ should be better than that of LiFePO$_4$. Therefore, the synthesis of Li$_2$MSiO$_4$ was considered a new potential polyanion cathode material for LiFePO$_4$ lithium batteries.

The capacity will be larger if the cathode material provides more reversible free electrons in the charge–discharge process [14]. The synthesis of Li$_2$MSiO$_4$ is considered as an ideal material that can provide multiple electrons. The synthesis of Li$_2$MSiO$_4$ can increase the valence of transition metal from + 2 to + 4 theoretically, which can separate two Li$^+$ reversibly in the charge process, eventually double the capacity of the cathode material. That is the reason researchers are interested in the material.

The crystal structure of Li$_2$FeSiO$_4$ is formed by linking tetrahedrons SiO$_4$, FeO$_4$, and LiO$_4$, in a similar fashion as LiFePO$_4$ [15]. SiO$_4$ and FeO$_4$ form the framework by connecting each other alternately on the same side, and Li$^+$ is located in the interlamination of the structure -SiO$_4$-FeO$_4$-SiO$_4$-FeO$_4$-. This means that the Li$^+$ is connected to SiO$_4$ and FeO$_4$ from the same point, and the intercalation and separation proceed from this location. Li$_2$FeSiO$_4$ was synthesized and analyzed by Yamada et al. [16] and was finally considered belongs to monoclinic system. Its point group was found to be *P21*, and with lattice parameters $a$ = 0.822898 nm, $b$ = 0.502002 nm, $c$ = 0.823335 nm, and $\beta$ = 99.2027(5)°, respectively. Although Li$_2$MSiO$_4$ can provide two electrons reversibly in the process of the intercalation and a separation theoretical redox couple (M$^{2+}$/M$^{3+}$ and M$^{3+}$/M$^{4+}$) [17], the second Li$^+$ requires quite high voltage to separate after the separation of the first one. The second Li$^+$ in Li$_2$CoSiO$_4$ needs more than

✉ Enshan Han
  eshan@hebut.edu.cn

1  School of Chemical Engineering and Technology, Hebei University of Technology, Tianjin 300130, People's Republic of China

5 V to achieve separation, which is beyond the upper limit of stability (4.5 V) of the electrolyte used in today's lithium batteries. Therefore, the separation of the second electron of the $Li_2MSiO_4$ is limited because of the voltage. In the process of initial charging, the space group of $Li_2FeSiO_4$ has changed into $P21$; then, the structure of the material remains stable, which provides a tube for insertion/extraction of lithium-ion. $Fe^{2+}$ is surrounded by $SiO_4$ which is formed by iron oxygen tetrahedron and silicon oxygen tetrahedron. $Fe^{2+}$ was separated from each other, so the ability of electronic conductivity and lithium-ion diffusion is very low.

Considering the low intrinsic electronic conductivity and slow lithium-ion diffusion ability of $Li_2FeSiO_4$, decreasing its particle size and coating it with high-conductivity materials are key points for improving the electrochemical performance of $Li_2FeSiO_4$ [18–20]. A literature review shows that Mg doping is apparently beneficial for improving the rate and cycle performances of phosphate cathode materials, such as $LiFePO_4$ and $Li_3V_2(PO_4)_3$, because Mg doping not only increases lithium-ion diffusion capability but also decreases charge–transfer resistance. Furthermore, Mg doping strengthens structural stability during the lithiation–delithiation [21–25]. Zhang et al. [26] have synthesized $Li_2Fe_{0.97}Mg_{0.03}SiO_4$ via a sol–gel method with soluble Li, Fe, Si, and Mg sources. Research shows that $Li_2Fe_{0.97}Mg_{0.03}SiO_4$ has a monoclinic structure and their lattice parameters are similar, which indicates that $Mg^{2+}$ has been doped into the structure of $Li_2FeSiO_4$ without destroying its lattice structure. Electrochemical impedance analysis shows that Mg doping decreases charge transfer resistance of $Li_2FeSiO_4$ and increases the lithium-ion diffusion coefficient of $Li_2FeSiO_4$. Qu et al. [27] have synthesized Mg-doped $Li_2FeSiO_4$/C by using $Fe_2O_3$

nanoparticle as iron source. Rietveld refinement confirms that Mg is doped in Fe site in $Li_2FeSiO_4$ lattice. This Mg-doped $Li_2FeSiO_4$/C product shows high capacity retention of 96% after 100 cycles at 0.1 C. It is concluded that Mg-doping can help in decreasing the charge-transfer resistance and increasing the lithium-ion diffusion capability.

In this paper, in order to establish the crystal structure and improve the cycling performance of $Li_2FeSiO_4$, the precursor of $Li_2Fe_{1-y}Mg_ySiO_4$/C ($y = 0$, 0.01, 0.02, 0.03, 0.05) was synthesized by the high temperature solid-state method, and then made into batteries to test their electrochemical properties. The source of magnesium was $MgC_4H_6O_4 \cdot 4H_2O$. The effects of $Mg^{2+}$ doping on the electrochemical performance of $Li_2FeSiO_4$ are discussed in detail. Our approach differs from that of Zhang et al. [26] in the following aspects: firstly, the synthetic methods are different. In this paper, the high-temperature solid-state method is adopted which is suitable for industrialization, but the sol–gel method is described in the literature. Secondly, the synthesis materials are different, ferric citrate is used in the literature, but $FeC_2O_4 \cdot 2H_2O$ is used in this paper. Finally, the synthesis samples of different amounts of Mg being added were compared and studied in this paper and the synthesis temperature and time have been optimized. The differences between our study and that of Qu et al. [27] are as follows: firstly, the synthesis materials are different, and they used the more expensive $Fe_2O_3$ nanoparticle; in this study, we used $FeC_2O_4 \cdot 2H_2O$ which is relatively cheap and easily available. Secondly, the discrepancies in electrochemical properties of the synthesized samples were discussed under different calcination temperatures and calcination time. The main studies described in the literature are the performance of Mg-doped materials (3 mol%) at low temperatures.
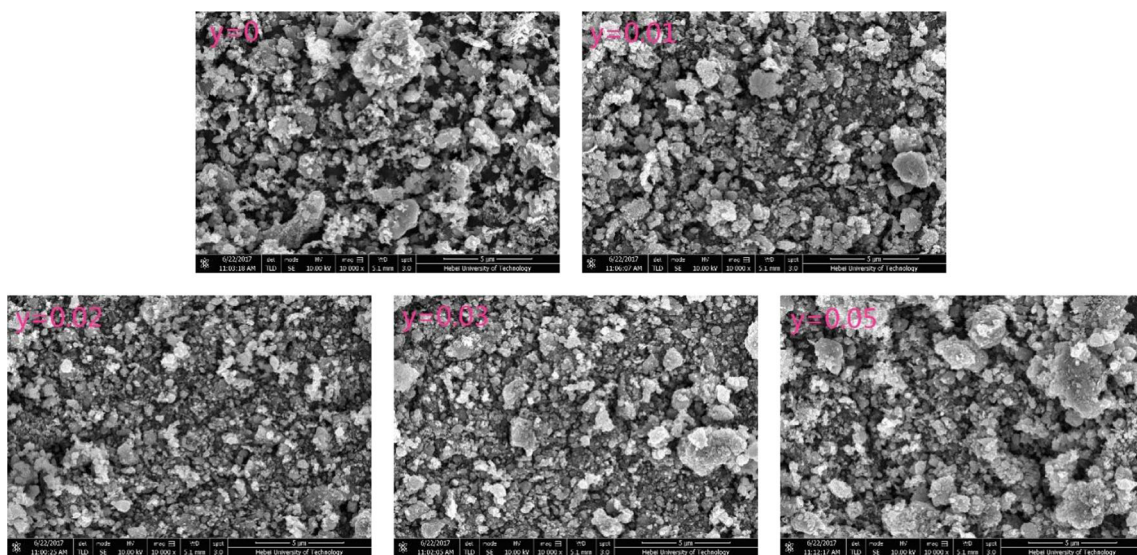


**Fig. 1** SEM images of $Li_2Fe_{1-y}Mg_ySiO_4$/C
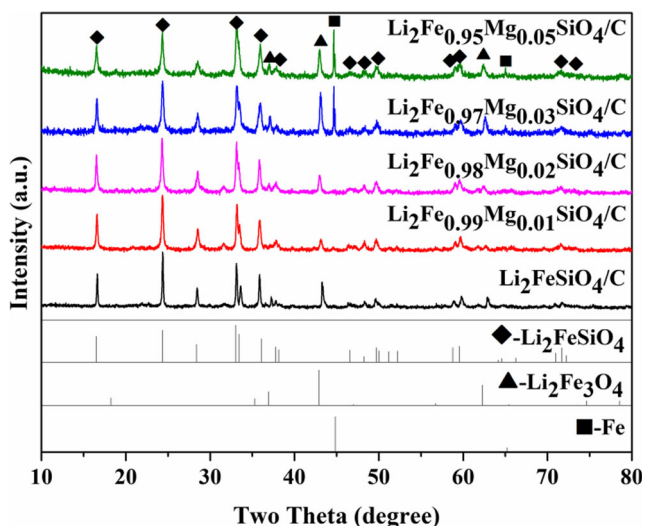
**Fig. 2** XRD patterns of $Li_2Fe_{1-y}Mg_ySiO_4/C$



**Fig. 3** Initial charge–discharge curves of $Li_2Fe_{1-y}Mg_ySiO_4/C$ at 0.1 C

## Experimental

### Synthesis

$Li_2Fe_{1-y}Mg_ySiO_4/C$ ($y = 0$, 0.01, 0.02, 0.03, 0.05) were prepared as follows: stoichiometric amounts of the lithium source ($CH_3COOLi$), iron source ($FeC_2O_4 \cdot 2H_2O$), silicon source (TEOS), carbon source (citric acid) (the molar mass of carbon to $Li_2FeSiO_4$ ratio is 1:10), and $MgC_4H_6O_4 \cdot 4H_2O$ were taken and ball milled with about 10 ml anhydrous alcohol as medium. The milling speed and time were controlled at 250 r min$^{-1}$ for 5 h, respectively. Then, the precursor was dried under 80 °C in oven and crushed in mortar. After that, the powder was preheated in tube furnace under $N_2$ atmosphere, at 350 °C for 5 h, then was crushed again about 30 min after cooling. Finally, the powder precursor was calcined under $N_2$ atmosphere at 700 °C for at least 10 h, and after natural cooling, the $Li_2Fe_{1-y}Mg_ySiO_4/C$ was obtained.

### Preparation of positive film and battery assembly

The active material, conductive carbon black, and polyvinylidene fluoride (PVDF) were taken in the weight of 8:1:1 and dissolved in the N-methyl-pyrrolidone (NMP). The slurry was covered over aluminum foil and then dried at 110 °C for 10 h in vacuum. After that, the electrode film was pressed and punched into a circular disk and the cathode electrodes were finished.

The CR2032 coin cell was used to test the electrochemical properties of the cathode electrodes mentioned above. The cell was made of a lithium metal electrode with a polypropylene microporous film (Celgard2300) in the middle.

The LiPF$_6$ (1 M) was used as electrolyte in dimethyl carbonate (DMC), ethyl methyl carbonate (EMC), and ethylene carbonate (EC), while the coin cells were installed in glove compartment.

Crystal structure of the syntheses was determined by X-ray diffraction (XRD) analyzer (D8-Fouse, made in Germany) with Cu-K$\alpha$ radiation, and the scanning range was 10°–90° while the scanning speed is 8° min$^{-1}$. The morphologies of the powders were analyzed by scanning electron microscope (SEM, Nova Nano SEM 450 FEI). The battery testing system

**Table 1** Lattice parameters of $Li_2Fe_{1-y}Mg_ySiO_4/C$

| $y$ | $a$ (Å) | $b$ (Å) | $c$ (Å) | $V$ (Å$^3$) |
|---|---|---|---|---|
| $y = 0$ | 8.2349415 | 5.0067280 | 8.2239445 | 334.65253 |
| $y = 0.01$ | 8.2315876 | 5.0090227 | 8.2354718 | 335.44462 |
| $y = 0.02$ | 8.2374310 | 5.0064739 | 8.2362674 | 335.62862 |
| $y = 0.03$ | 8.2262574 | 4.9995892 | 8.2324488 | 334.49045 |
| $y = 0.05$ | 8.2340107 | 4.9952579 | 8.2357293 | 334.78414 |



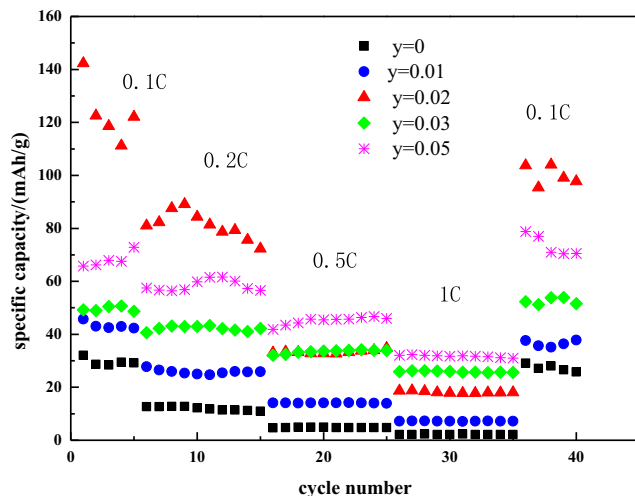**Fig. 4** Cycle performance of $Li_2Fe_{1-y}Mg_ySiO_4/C$ at different rate

Land CT2001A was used to evaluate the constant current charge and discharge, and the voltage ranges from 1.5 to 4.8 V.

The cyclic voltammetry (CV) was performed on a CHI660C electrochemical analyzer; the voltage range was 1.7–4.0 V (versus Li$^+$/Li) with a scanning rate of 0.1 mV s$^{-1}$. The electrochemical impedance spectroscopy (EIS) was also accomplished on the same analyzer, by varying the frequency from 100 kHz to 0.01 Hz, while the AC amplitude was 5 mV. The software ZsimpWin 3.10 was used to analyze the EIS data.

## Results and discussion

### Physical characteristics

The SEM images of the Li$_2$Fe$_{1-y}$Mg$_y$SiO$_4$/C composites are shown in Fig. 1. All the samples present similar morphology, and the powders consist of agglomerates of primary particles. As can be seen, when $y = 0.02$, the particle morphology of the images are smaller in particle size, and well-distributed, which is conducive to shorten the lithium diffusion distance, and the loosely distributed small particles decrease, indicating that the introduction of Mg$^{2+}$ has promoted the agglomeration of particles. There are large particles in the sample without doped Mg atoms. While the sample has obvious agglomeration with increased $y$; apparently, the particles become larger when $y = 0.03$ and 0.05.

XRD patterns of all samples are shown in Fig. 2. A full refinement was carried out showing that the dominant crystal phase of all the samples is the monoclinic structure $P21/n$. It can be seen from Fig. 2 that all of the diffraction peaks are sharp, which means the degree of crystallinity is good.

A few of impurities of Li$_2$Fe$_3$O$_4$ were detected by the peaks at 42.8°. The intensity of the peak is the lowest as $y$ increases



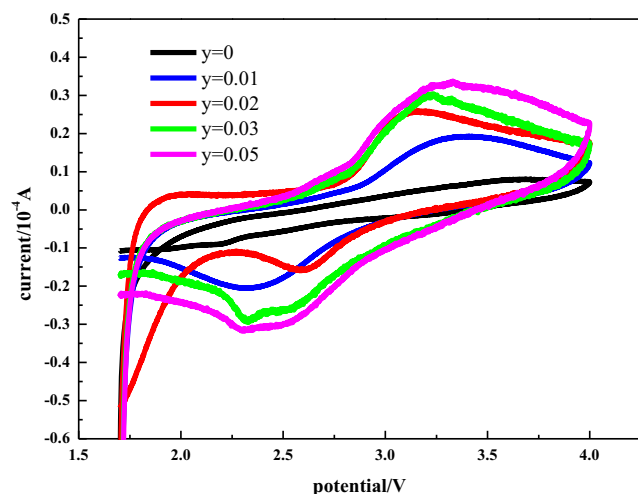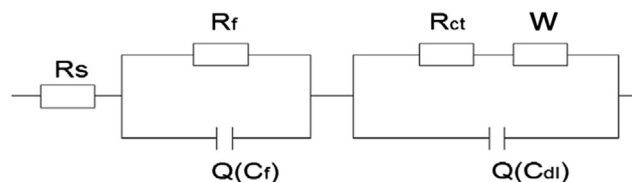**Fig. 6** Equivalent circuit for fitting of EIS

to 0.02 and higher when $y = 0.03$ and 0.05. The lattice stability of the material is affected when the Mg content increases, leading to the generation of impurities. When $2\theta$ is 44.6°, this reflection matches the (001) characteristic peak of metallic iron, reported as an impurity phase in Li$_2$FeSiO$_4$/C material prepared via a solid-state reaction process [28]. The occurrence of the Fe peak is because a little Fe$^{2+}$ was reduced to ferric elemental state by the carbon produced during the calcination of citric acid. That shows the crystal lattices of the sample become instable when $y$ is above 0.02, and finally leads to the reduction of ferric ion. Table 1 shows the lattice parameters of Li$_2$Fe$_{1-y}$Mg$_y$SiO$_4$/C. We can see from Table 1 that the lattice volume changes little when $y = 0.01$ and 0.02, which means the Mg$^{2+}$ was doped into the lattices successfully. When $y = 0.03$ and 0.05, more iron impurities were precipitated and the lattice constant $b$ is decreased a little, showing that the lattices will shrink once excessive ferric ion was replaced by Mg$^{2+}$ [29]. The XRD patterns of samples can be indexed to a monoclinic structure in space group $P21$. Mg$^{2+}$ doping does not destroy the lattice structure of Li$_2$FeSiO$_4$ because of the low doping concentration [26]. However, the peaks of the Li$_2$FeSiO$_4$ shift to lower diffraction angles after Mg doping, which indicates the lattice parameters change when $y = 0.03$, 0.05. The lattice parameters decrease after Mg$^{2+}$ doping, which can be attributed to the smaller atomic size of Mg$^{2+}$ (0.66 Å) than Fe$^{2+}$ (0.74 Å) or Li$^+$ (0.76 Å) [30].
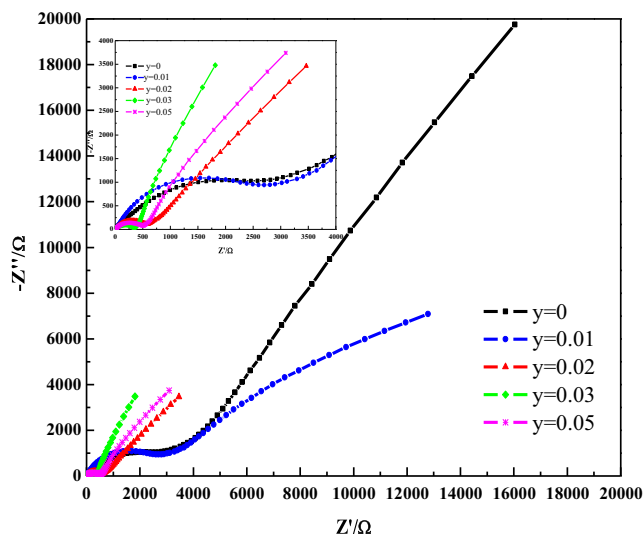


**Fig. 5** CV curves of Li$_2$Fe$_{1-y}$Mg$_y$SiO$_4$/C



**Fig. 7** Electrochemical impedance spectroscopy (EIS) of Li$_2$Fe$_{1-y}$Mg$_y$SiO$_4$/C
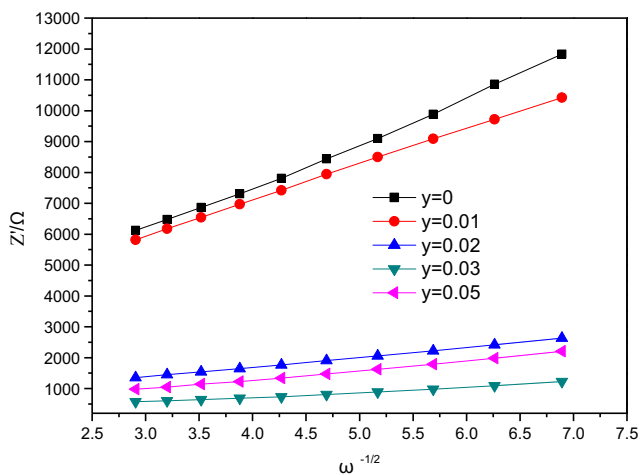
**Fig. 8** linear fitting of the $Z'$ versus $\omega^{-1/2}$ relationship of $Li_2Fe_{1-y}Mg_ySiO_4/C$

## Electrochemical characteristics

From Fig. 3, we can see that when the $y$ minus 0, 0.01, 0.02, 0.03, and 0.05 separately, the first discharge capacity is 32.1, 45.7, 142.3, 49.2, and 65.8 mAh g$^{-1}$, respectively, and the coulombic efficiency is 51.3, 54.3, 95.6, 45.9, and 46.4% correspondingly. In addition with the previous analysis, when $y = 0, 0.01$, the direct cause of lower discharge capacity is that the particles of material are bigger, and when $y = 0.03, 0.05$, based on the results of XRD analysis, cell volume of material is shrinking, which leads to a more impurity phase and the discharge capacity is also affected. It is suggested that the formation of Fe and the reduced agglomeration of the particles diminishes resistance towards Li$^+$ ions and electron mobility; hence, this stabilizes the charge-discharge cycling performance [31]. Pure phase material has small capacity because its voltage changes quickly and unsteadily in the charge–discharge process. The discharge capacity is less than charge capacity when $y = 0.01, 0.03$, and 0.05, which indicate that the intercalation and separation of Li$^+$ is incomplete during the charge–discharge process. As can be seen from Fig. 4, the voltage of the undoped material changes rapidly in the initial stage of the charge and discharge, the voltage of the material doped with Mg changes slowly. Especially, when $y = 0.02$, the voltage platform is longer and the electrode

polarization is smaller. The discharge capacity is large and the voltage platform is steady when $y = 0.02$, which shows that the electrochemical property of the material is better. It is because the doped Mg atoms replace some Fe atoms in the lattice, thus decreases the trans effect between Li and Fe and increases the diffusion ability of Li$^+$; compared with the undoped material, the electrochemical performance is improved [27]. When the dopant content continues to increase, the amount of impurities will increase, which affects the improvement of the electrochemical performance.

Figure 4 shows that the rate property of the $Li_2FeSiO_4$ with different proportion of Mg atoms are all good, indicating the doping of Mg atom benefits to structural stability. Especially, the synthesis with $y = 0.02$ has the highest specific capacity at low rate. Even though a little lower at high rate, it still has a significant rate property as a whole, and the capacity retention ratio after cycle is 68.7%. The attenuation of capacity is mainly determined by the side reaction between electrolyte and electrode, as well as how steady the crystal structure is in the charge–discharge process. Because of the doped Mg atoms, parts of the Fe atoms are replaced and that may suppress the side reaction mentioned above. The polymorph changes from monoclinic to orthorhombic structure during the first few cycles; as can be seen in Fig. 4, the initial cycles are unstable when $y = 0.02$. Meanwhile, the cell volume of $Li_2FeSiO_4$ shrinks for the same reason [30], may contribute to reducing the change of lattice volume in the charge–discharge process, and makes the crystal structure steadier.

Figure 5 is cyclic voltammetry for the $Li_2FeSiO_4$ with different proportion of Mg atoms. With the increase of the value of $y$, the redox peaks are clearer and clearer, the peak areas are getting bigger and bigger, and the symmetry of redox peaks is good. When $y = 0.02$, the potential difference of the redox peaks is minimum. The peak potentials are 2.58 and 3.12 V respectively, and the difference is 0.54 V. That means electrode polarization is minimum in the charge–discharge process when $y = 0.02$. The peak in the CV curve is not clear when $y = 0$, which means the charge and discharge capacity of materials is poor. Although the peak is clear when $y = 0.01, 0.02$, and 0.05, the distance between oxidation and reduction peaks is large. We can see from the first charge–discharge curve that the electrode polarization upon doping improves the

**Table 2** EIS fitting data of $Li_2Fe_{1-y}Mg_ySiO_4/C$

| Samples | $R_s$ (Ω) | $Q(C_f)$ (F) | $R_f$ (Ω) | $Q(C_{dl})$ (F) | $R_{ct}$ (Ω) | $W/\Omega/s^{1/2}$ | $D_{Li}^+$ (cm$^2$ s$^{-1}$) |
|---|---|---|---|---|---|---|---|
| $Li_2FeSiO_4/C$ | 1.219 | $1.376 \times 10^{-5}$ | 3289 | $2.174 \times 10^{-4}$ | $4.655 \times 10^4$ | $7.362 \times 10^{-6}$ | $1.842 \times 10^{-17}$ |
| $y = 0.01$ | 3.656 | $6.405 \times 10^{-6}$ | 2337 | $2.318 \times 10^{-4}$ | $5.708 \times 10^4$ | 91.96 | $2.817 \times 10^{-17}$ |
| $y = 0.02$ | 5.719 | $9.832 \times 10^{-6}$ | 579 | $6.454 \times 10^{-4}$ | 869.7 | $4.282 \times 10^{-4}$ | $3.710 \times 10^{-16}$ |
| $y = 0.03$ | 2.709 | $9.019 \times 10^{-6}$ | 350.9 | $1.952 \times 10^{-3}$ | 0.01002 | $2.867 \times 10^{-16}$ | $1.407 \times 10^{-15}$ |
| $y = 0.05$ | 3.954 | $1.455 \times 10^{-5}$ | 501.4 | $1.207 \times 10^{-3}$ | $3.737 \times 10^4$ | $6.084 \times 10^{-3}$ | $3.975 \times 10^{-16}$ |
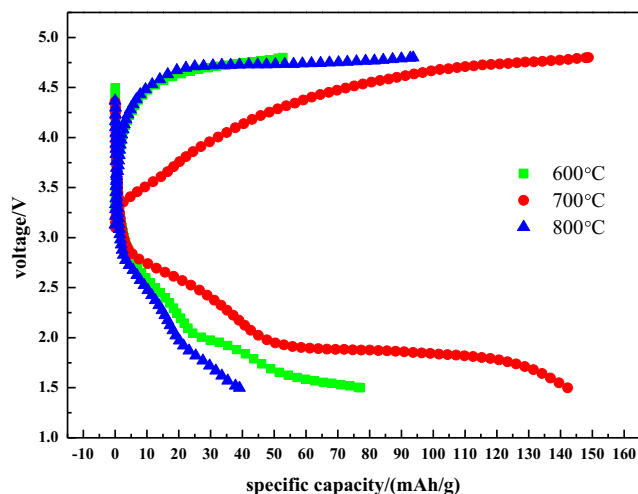
**Fig. 9** Initial charge–discharge curves of $Li_2Fe_{0.98}Mg_{0.02}SiO_4/C$ synthesized at 600, 700, and 800 °C



**Fig. 11** CV curves of $Li_2Fe_{0.98}Mg_{0.02}SiO_4/C$ synthesized at 600, 700, and 800 °C

reversibility. Combining with the XRD analysis, there is more than a single pair of cathodic/anodic peaks (one $Fe^{2+}/Fe^{3+}$ redox couple) in the sample. The occurrence of impurities is quite large and they may be electro active. From the peak areas, the deintercalation–intercalation by $Li^+$ ions is favored by doping.

Figure 7 is an AC impedance diagram compared among the $Li_2FeSiO_4$ with different proportion of Mg atoms. It shows the doping with Mg atoms change the impedance significantly. All EIS curves were fitted by an equivalent circuit composed of "R(QR)(Q(RW))" (in Fig. 6) using the ZSimpWin program, and the fitting results are shown in Table 2. Here, $R_s$, $R_f$, and $R_{ct}$ are resistances of the electrolyte, the interface electric resistance, and the charge transfer reaction, respectively. The capacitance of the SEI film and the capacitance of the double layer are represented by the constant-phase elements Q ($C_f$) and Q ($C_{dl}$), and the quasi-straight line at low-frequency region represents the
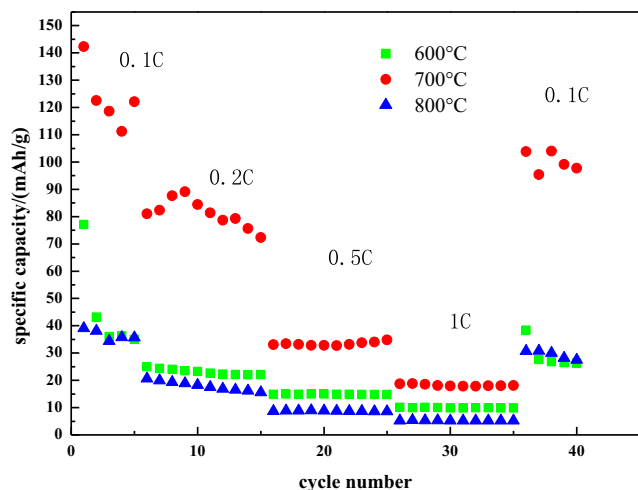
Warburg impedance (W) related to the impedance of $Li^+$ diffusion in bulk material (Fig. 7).

$$D_{Li^+} = \frac{R^Z \cdot T^Z}{2A^Z \cdot n^Z \cdot F^4 \cdot C^Z \cdot \sigma^Z} \tag{1}$$

The linear fitting of $Z'$ vs. $\omega^{-1/2}$ in the low-frequency region of $Li_2Fe_{1-y}Mg_ySiO_4/C$ samples is shown in Fig. 8. In high-frequency region, the values of charge transfer resistance ($R_{ct}$) are small, in these cases when $y = 0.02$ and 0.03, thus benefits to the intercalation and separation of $Li^+$. When $y = 0.01$, it shows that the Warburg resistance (W) is large under these circumstances. The lithium-ion diffusion coefficients ($D_{Li+}$) of $Li_2Fe_{1-y}Mg_ySiO_4/C$ are calculated according to the equivalent circuit and lithium-ion diffusion coefficients (Eq. (1)) [32], where R is the gas constant (8.314 J $mol^{-1}$ $K^{-1}$), T is the absolute temperature, A is the surface area of the



**Fig. 10** Cycle performance at different rate of $Li_2Fe_{0.98}Mg_{0.02}SiO_4/C$ synthesized at 600, 700, and 800 °C



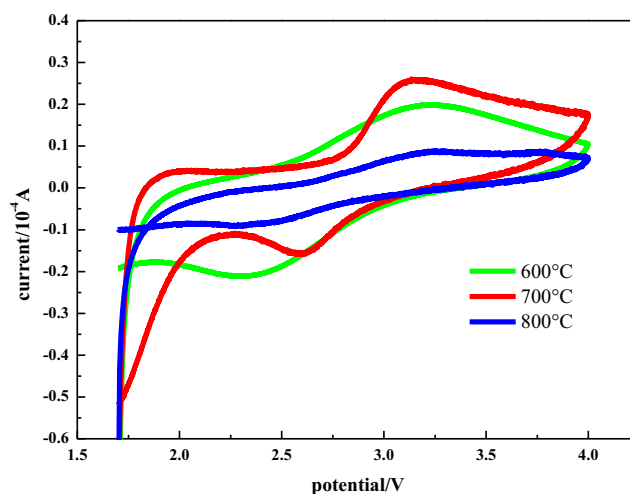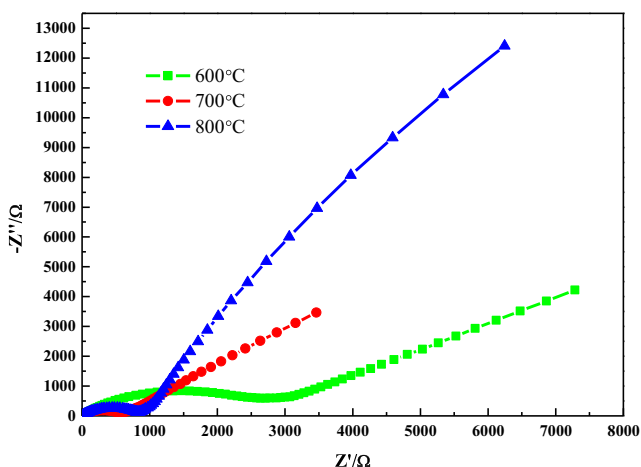**Fig. 12** Electrochemical impedance spectroscopy (EIS) of $Li_2Fe_{0.98}Mg_{0.02}SiO_4/C$ synthesized at 600, 700, and 800 °C
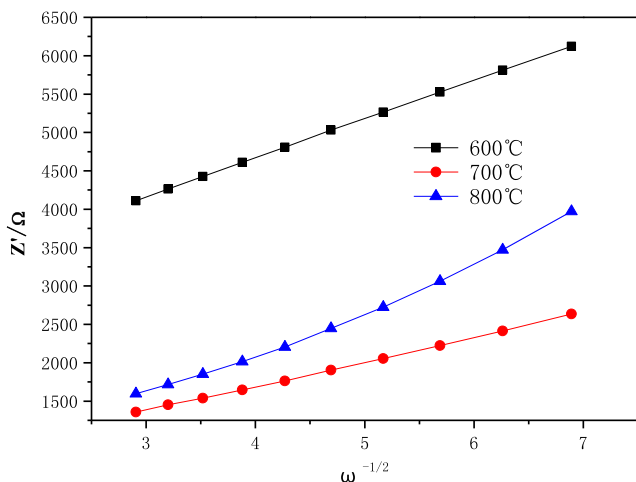
**Fig. 13** Linear fitting of the $Z'$ versus $\omega^{-1/2}$ relationship of $Li_2Fe_{0.98}Mg_{0.02}SiO_4/C$ synthesized at 600, 700, and 800 °C



**Fig. 14** Initial charge–discharge curves of $Li_2Fe_{0.98}Mg_{0.02}SiO_4/C$ with different calcining time

cathode (here A was estimated to be the surface area of electrode, 0.785cm$^2$), $n$ is the number of electrons per molecule during oxidation, $F$ is the Faraday constant (96,485.33 C mol$^{-1}$), $C$ is the bulk concentration of Li$^+$ in the electrode (0.0390 mol cm$^{-3}$ for $Li_2FeSiO_4$ [33]), and $\sigma$ is the Warburg factor (the rake ratio of Fig. 8). It can be seen from the Table 2 that, compared with the other samples, the $D_{Li+}$ of the syntheses when $y = 0.02$, 0.03, and 0.05 is one order higher than the syntheses with the $y = 0$ and 0.01. Combined with the CV curve and the first charge–discharge curve, it can be seen that the oxidation and reduction peaks are both sharp while the distance between them is large, and the charge capacity is much larger than discharge capacity when $y = 0.03$. Therefore, although when $y = 0.03$, the $D_{Li+}$ is high, and the $R_{ct}$ is low, the reversibility is poor, which affects the electrochemical property of the material significantly. The lithium-ion diffusion coefficient of $Li_2Fe_{0.97}Mg_{0.03}SiO_4/C$ is greater than $Li_2Fe_{0.98}Mg_{0.02}SiO_4/C$, but its $R_{ct}$ is very small and not in a normal range. From Figs. 3 and 4, it shows that the coulombic efficiency and capacity of $Li_2Fe_{0.97}Mg_{0.03}SiO_4/C$ are relatively poor, so it could not only judge the quality of the material from the lithium-ion diffusion coefficient but also depends on results of many different tests. In combination with the specific capacity, rate property, and cyclic voltammetry, the sample with $y = 0.02$ has better electrochemical properties on the whole, and this proportion of doped Mg atoms is the best to improve the diffusion
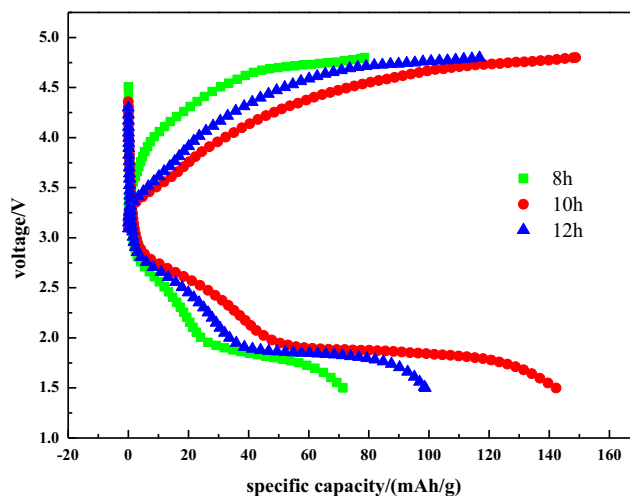
capability of lithium-ion in $Li_2FeSiO_4$; the effect of Mg doping on the electronic conductivity of the $Li_2FeSiO_4/C$ sample is insignificant [26].

## The optimization of conditions for the synthesis of Li$_2$FeSiO$_4$

From the foregoing point of view, when $y = 0.02$, the material has the highest specific capacity. So, at first, we investigated the effect of calcination temperature on electrochemical property of the synthesis $Li_2Fe_{0.98}Mg_{0.02}SiO_4/C$. The temperature was set at 600, 700, and 800 °C, respectively, and the calcination time is 10 h.

It can be seen from Figs. 9 and 10 that the first discharge capacities are 77.1, 142.3, and 39.1 mAh g$^{-1}$ correspondingly when calcination temperature is 600, 700, and 800 °C, respectively. The rate property curves indicate that the specific discharge capacity is the highest when the synthesis calcination is at 700 °C: after charge–discharge cycles under 0.1, 0.2, 0.5, 1, and 0.1 C successively, the capacity is 97.7 mAh g$^{-1}$ under the last 0.1 C, and the retention rate is 68.7%.When the calcination temperature is 600 and 800 °C, the electrochemical properties of the materials are poor; especially, when the temperature is 800 °C, the discharge capacity of is only 39.1 mAh g$^{-1}$ at 0.1 C. The excessive temperature contributes to increasing the grain size of $Li_2FeSiO_4$, which blocks the diffusion of

**Table 3** EIS fitting data of $Li_2Fe_{0.98}Mg_{0.02}SiO_4/C$ synthesized at 600, 700, and 800 °C

| Samples | $R_s$ (Ω) | Q($C_f$) (F) | $R_f$ (Ω) | Q ($C_{dl}$) (F) | $R_{ct}$ (Ω) | W/Ω/s$^{1/2}$ | $D_{Li}^+$ (cm$^2$ s$^{-1}$) |
|---------|-----------|--------------|-----------|------------------|--------------|----------------|------------------------------|
| 600 °C  | 3.728     | $8.937 \times 10^{-6}$ | 2492 | $2.765 \times 10^{-4}$ | 208.1 | $2.623 \times 10^{-4}$ | $1.483 \times 10^{-16}$ |
| 700 °C  | 5.719     | $9.832 \times 10^{-6}$ | 579  | $6.454 \times 10^{-4}$ | 869.7 | $4.282 \times 10^{-4}$ | $3.710 \times 10^{-16}$ |
| 800 °C  | 4.839     | $7.585 \times 10^{-6}$ | 871.6 | $5.546 \times 10^{-4}$ | $2.648 \times 10^{5}$ | $7.264 \times 10^{-4}$ | $1.091 \times 10^{-16}$ |
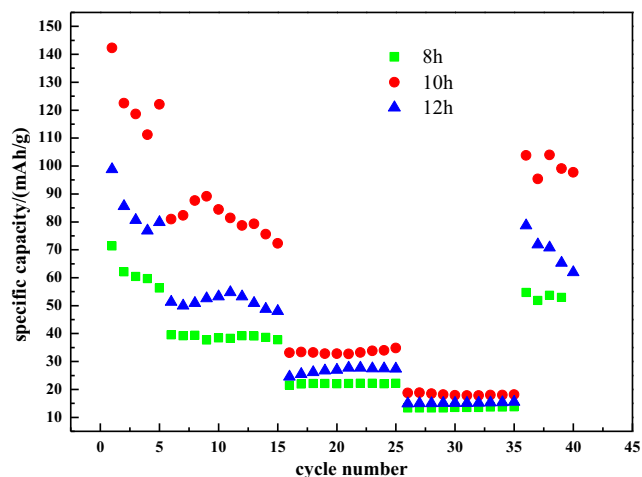
Fig. 15 Cycle performance at different rate of Li$_2$Fe$_{0.98}$Mg$_{0.02}$SiO$_4$/C with different calcining time



Fig. 17 Electrochemical impedance spectroscopy (EIS) of Li$_2$Fe$_{0.98}$Mg$_{0.02}$SiO$_4$/C with different calcining time

Li$^+$ in the lattice. Besides, the carbon coating on the surface of the synthesized material can be burned by the high temperature, decreasing its beneficial effect [34].

Figure 11 shows the CV curves of Li$_2$Fe$_{0.98}$Mg$_{0.02}$SiO$_4$/C synthesized at 600, 700, and 800 °C. The sample annealed at 600 °C were clearly identified as the Li$_2$FeSiO$_4$ phase with the space group *P21* from the results reported by Nishimura et al. [16]. We can see that the redox peak is the clearest as well as the potential difference of the peaks is minimum at 700 °C, while there is hardly any redox peak at 800 °C. Sample obtained at 800 °C was refined in the *P21* space group [35]. All the crystallographic sites were constrained to be fully occupied. The isotropic atomic thermal displacement parameters (B$_{iso}$) were fixed to 1.0, 0.96, 0.49, and 0.51 Å$^2$ for lithium, iron, silicon, and oxygen, respectively. This refinement revealed that cell and structural parameters are very close to those reported by Nishimura et al. [16] ($a = 8.230(2)$ Å, $b = 5.0216(2)$ Å, $c = 8.234(2)$ Å, and $\beta = 99.232°(3)$), but we used
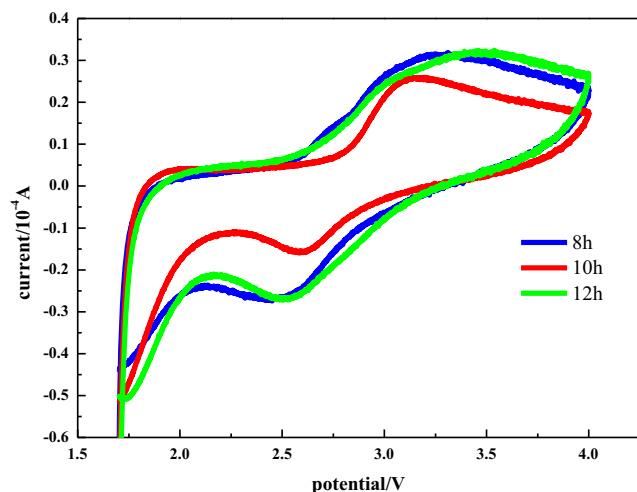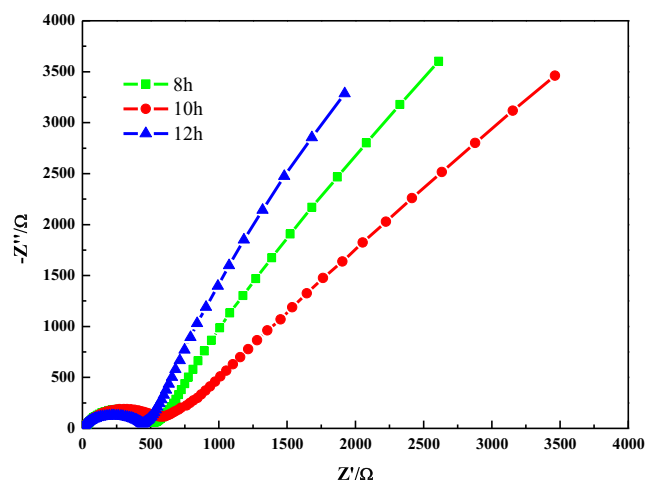
the *P21/n* space group instead of *P21*, following Yamada's recent oral communication [36].

When calcination temperature is 600 °C, the peak potential differences are bigger than 700 °C. It indicates that the electrode polarization is few in the charge–discharge process, and the reversibility of the electrode is good when the synthesis was calcination at 700 °C, while the diffusion of Li$^+$ is blocked and the electrical conductivity is reduced if calcination at 800 °C.

We can see from the Figs. 12 and 13 and combined with Table 3, when sample is calcined at 600 and 700 °C, the charge transfer resistance (R$_{ct}$) is far less than when it is calcined at 800 °C, indicating that if the temperature is too high, the charge transfer resistance of the material will obviously increase, thus does not benefit the intercalation and separation of Li$^+$. The D$_{Li+}$ of the synthesis calcination under700 °C is higher than its under 600 and 800 °C. It may be concluded that the best annealing temperature is 700 °C.



Fig. 16 CV curves of Li$_2$Fe$_{0.98}$Mg$_{0.02}$SiO$_4$/C with different calcining time
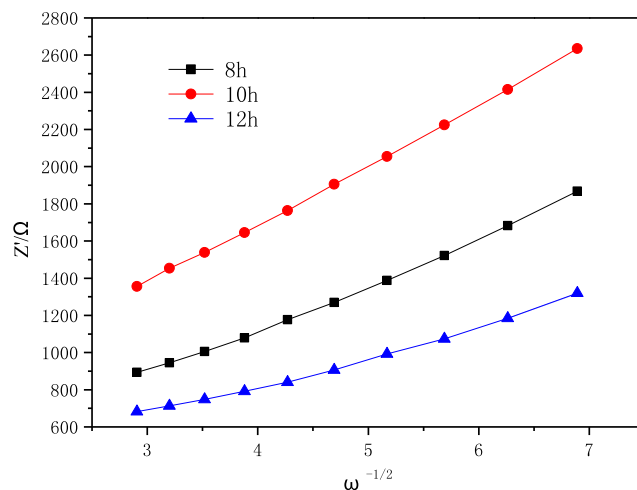


Fig. 18 Electrochemical impedance spectroscopy (EIS) of Li$_2$Fe$_{0.98}$Mg$_{0.02}$SiO$_4$/C with different calcining time

**Table 4** EIS fitting data of $Li_2Fe_{0.98}Mg_{0.02}SiO_4/C$ with different calcining time

| Samples | $R_s$ (Ω) | $Q(C_f)$ (F) | $R_f$ (Ω) | $Q(C_{dl})$ (F) | $R_{ct}$ (Ω) | $W/\Omega/s^{1/2}$ | $D_{Li}^+$ (cm$^2$ s$^{-1}$) |
|---|---|---|---|---|---|---|---|
| 8 h | 8.136 | $9.717 \times 10^{-6}$ | 554.9 | $1.232 \times 10^{-3}$ | 729 | $4.349 \times 10^{-4}$ | $6.352 \times 10^{-16}$ |
| 10 h | 5.719 | $9.832 \times 10^{-6}$ | 579 | $6.454 \times 10^{-4}$ | 869.7 | $4.282 \times 10^{-4}$ | $3.710 \times 10^{-16}$ |
| 12 h | 2.402 | $8.535 \times 10^{-6}$ | 435.7 | $1.953 \times 10^{-3}$ | 4720 | $5.612 \times 10^{-19}$ | $1.507 \times 10^{-15}$ |

On the basis of the best calcination temperature (700 °C), we investigated the electrochemical property of the syntheses which were calcined for 8, 10, and 12 h, respectively, and found the best calcination time. The relative stability and electrochemical properties of various $Li_2FeSiO_4$ polymorphs were very recently investigated from first-principle calculations [37]. All of them were shown to have very similar energies, which explain the difficulties to control the synthesis of single-phase samples of $Li_2FeSiO_4$ polymorphs but also very similar electrochemical properties (voltage, volume variation, and electronic structure) [38].

From Figs. 14 and 15, we can see that the first discharge capacity is 71.4, 142.3, and 98.8 mAh g$^{-1}$ correspondingly when the time is 8, 10, and 12 h, respectively. Figure 15 shows that the specific capacity of the synthesis calcination for 10 h is always higher than the synthesis calcination for 8 or 12 h. At the end of the cycle, the capacities of synthesis calcination for different time are 74.1, 68.7, and 62.7% of the initial capacity, respectively.

Figure 16 shows that the peak positions and the peak areas are both closed to each other on the voltammetry curves for the synthesis calcination for 8 and 12 h, but the shapes of the peaks are not clear or sharp enough while the symmetry is poor and the potential difference of redox peaks is large. The redox peak is clear, and the potential difference of peaks is small when calcined for 10 h, indicating that the electrode polarization is minimum in the charge–discharge process and the reversibility of the electrode is good in this case.

It can be seen from the Figs. 17 and 18 and Table 4 that in the high-frequency region, when calcination time is 12 h, both values of charge transfer resistance ($R_{ct}$) and the Warburg resistance (W) are bigger than other two samples. We can see from Figs. 14 and 15 that although the $D_{Li+}$ of the syntheses calcined for 8 and 12 h is a little higher than the synthesis calcination for 10 h, the distance between the peaks in CV curve and the first discharge capacity is smaller than discharge capacity, which indicates that the reversibility of the synthesis is poor. Therefore, 10 h is still recognized as the best calcination time.

## Conclusions

$Li_2Fe_{1-y}Mg_ySiO_4/C$ ($y = 0$, 0.01, 0.02, 0.03, 0.05) powders were prepared via solid-state reaction. The results showed that $Li_2Fe_{0.98}Mg_{0.02}SiO_4/C$ has higher specific capacity and better cycle stability as well as lower impedance and better reversibility. According to the data, the crystallinity of the syntheses is good and the particles are distributed uniformly, which are beneficial to reduce the change of lattice volume in the charge–discharge process and finally improve the stability of the crystal structure. We can see from the CV curve and ELS curve that the reversibility of the synthesis is good as well as the diffusion coefficient of the lithium-ion is higher than the pure phase material. We synthesize $Li_2Fe_{0.98}Mg_{0.02}SiO_4/C$ at different calcination temperature and time. Through data analysis, we can see that, in order to get the synthesis $Li_2Fe_{0.98}Mg_{0.02}SiO_4/C$ which has the best electrochemical property, the calcination temperature should be set at 700 °C, and the time should be 10 h. According to the study, the material $Li_2Fe_{0.98}Mg_{0.02}SiO_4/C$ has the best electrochemical performance, which shows initial discharge specific capacity of 142.3 mAh g$^{-1}$ at 0.1 C and coulomb efficiency of 95.6%, under the condition that the temperature is 700 °C and the annealing time is 10 h.

## References

1. Nyten A, Abouimrane A, Armand M, Gustafsson T, Thomas JO (2005) Electrochemical performance of $Li_2FeSiO_4$ as a new Li-battery cathode material. Electrochem Commun 7:156–160. https://doi.org/10.1016/j.elecom.2004.11.008
2. Dominko R, Bele M, Gaberscek M, Meden A, Remskar M, Jamnik J (2006) Structure and electrochemical performance of $Li_2MnSiO_4$ and $Li_2FeSiO_4$ as potential Li-battery cathode materials. Electrochem Commun 8(2):217–222. https://doi.org/10.1016/j.elecom.2005.11.010
3. Lyness C, Delobel B, Armstrong AR, Bruce PG (2007) The lithium intercalation compound $Li_2MnSiO_4$ and its behaviour as a positive electrode for lithium batteries. Chem Commun 46:4890–4892. https://doi.org/10.1039/B711552K
4. Dominko R, Bele M, Kokalj A, Gaberscek M, Jamnik J (2007) $Li_2MnSiO_4$ as a potential Li-battery cathode material. J Power Sources 174(2):457–461. https://doi.org/10.1016/j.jpowsour.2007.06.188
5. Arroyo-de Dompablo ME, Dominko R, Gallardo-Amores JM, Dupont L, Mali G, Ehrenberg H, Jamnik J, Moran E (2008) On the energetic stability and electrochemistry of $Li_2MnSiO_4$ polymorphs. Chem Mater 20:5574–5584. https://doi.org/10.1021/cm801036k
6. Arroyo-de Dompablo ME, Armand M, Tarascon JM, Amador U (2006) On-demand design of polyoxianionic cathode materials based on electronegativity correlations: an exploration of the $Li_2MSiO_4$ system (M=Fe, Mn, Co, Ni). Electrochem Commun 8(8):1292–1298. https://doi.org/10.1016/j.elecom.2006.06.003

7. Arroyo-de Dompablo ME, Amador U, Gallardo-Amores JM, Moran E, Ehrenberg H, Dupont L, Dominko R (2009) Polymorphs of Li$_3$PO$_4$ and Li$_2$MSiO$_4$ (M=Mn, Co). J Power Sources 189(1):638–642. https://doi.org/10.1016/j.jpowsour.2008.09.066

8. Nadherna M, Dominko R, Hanzel D, Reiter J, Gaberscek M (2009) Electrochemical behavior of Li$_2$FeSiO$_4$ with ionic liquids at elevated temperature. J Electrochem Soc 156(7):A619–A626. https://doi.org/10.1149/1.3133183

9. Dominko R, Conte DE, Hanzel D, Gaberscek M, Jamnik J (2008) Impact of synthesis conditions on the structure and performance of Li$_2$FeSiO$_4$. J Power Sources 178(2):842–847. https://doi.org/10.1016/j.jpowsour.2007.07.064

10. Dominko R, Arcon I, Kodre A, Hanzel D, Gaberscek M (2009) In-situ XAS study on Li$_2$MnSiO$_4$ and Li$_2$FeSiO$_4$ cathode materials. J Power Sources 189(1):51–58. https://doi.org/10.1016/j.jpowsour.2008.11.077

11. Gong ZL, Li YX, Yang Y (2007) Synthesis and electrochemical performance of Li$_2$CoSiO$_4$ as cathode material for lithium ion batteries. J Power Sources 174:524–527

12. Nyten A, Kamali S, Haggstrom L, Gustafsson T, Thomas JO (2006) The lithium extraction/insertion mechanism in Li$_2$FeSiO$_4$. J Mater Chem 16:2266–2272. https://doi.org/10.1039/B601184E

13. Nyten A, Stjerndahl M, Rensmo H, Siegbahn H, Armand M, Gustafsson T, Edstrom K, Thomas JO (2006) Surface characterization and stability phenomena in Li$_2$FeSiO$_4$studied by PES/XPS. J Mater Chem 16:3483–3488. https://doi.org/10.1039/B605578H

14. Gong ZL, Yang YJ (2011) Recent advances in the research of polyanion-type cathode materials for Li-ion batteries. Energy Environ Sci 4:3223–3242. https://doi.org/10.1039/C0EE00713G

15. Arroyo de Dompablo ME, Amador U, Gallardo-Amores JM et al (2009) Polymorphs of Li$_3$PO$_4$ and Li$_2$MSiO$_4$ (M=Mn, Co). J Power Sources 189(1):638–642. https://doi.org/10.1016/j.jpowsour.2008.09.066

16. Nishimura SI, Hayase S, Yamada A (2008) Structure of Li$_2$FeSiO$_4$. J Am Chem Soc 130(40):13212–13213. https://doi.org/10.1021/ja805543p

17. Arroyo de Dompablo ME, Armand M, Tarascon JM et al (2006) On-demand design of polyoxianionic cathode materials based on electronegativity correlations: an exploration of the Li$_2$MSiO$_4$ system (M=Fe, Mn, Co, Ni). J Electrochem Commun 8(8):1292–1298. https://doi.org/10.1016/j.elecom.2006.06.003

18. Dominko R (2008) Li$_2$MSiO$_4$ (M=Fe and/or Mn) cathode materials. J Power Sources 184(2):462–468. https://doi.org/10.1016/j.jpowsour.2008.02.089

19. Yamada A, Chung SC, Hinokuma K (2001) Optimized LiFePO$_4$ for lithium battery cathodes. J Electrochem Soc 148(3):A224–A229. https://doi.org/10.1149/1.1348257

20. Huang H, Yin S-C, Nazar LF (2001) Approaching theoretical capacity of LiFePO$_4$ at room temperature at high rates. Electrochem Solid State Lett 4:A170–A172

21. Wang B, Xu B, Liu T, Liu P, Guo C, Wang S, Wang Q, Xiong Z, Wang D, Zhao XS (2014) Mesoporous carbon-coated LiFePO$_4$ nanocrystals co-modified with graphene and Mg$^{2+}$ doping as superior cathode materials for lithium ion batteries. Nano 6(2):986–995. https://doi.org/10.1039/c3nr04611g

22. Ni J, Zhao Y, Chen J, Gao L, Lu L (2014) Site-dependent electrochemical performance of Mg doped LiFePO$_4$. Electrochem Commun 44:4–7. https://doi.org/10.1016/j.elecom.2014.04.004

23. Yang MR, Ke WH (2008) The doping effect on the electrochemical properties of LiFe$_{0.95}$M$_{0.05}$PO$_4$ (M=Mg$^{2+}$, Ni$^{2+}$, Al$^{3+}$, or V$^{3+}$) as cathode materials for lithium-ion cells. J Electrochem Soc 155(10):A729–A732. https://doi.org/10.1149/1.2960933

24. Meethong N, Kao Y-H, Speakman SA, Chiang Y-M (2009) Aliovalent substitutions in olivine lithium iron phosphate and impact on structure and properties. Adv Funct Mater 19(7):1060–1070. https://doi.org/10.1002/adfm.200801617

25. Huang JS, Yang L, Liu KY, Tang YF (2010) Synthesis and characterization of Li$_3$V$_{(2−2x/3)}$Mg$_x$(PO$_4$)$_3$/C cathode material for lithium-ion batteries. J Power Sources 195(15):5013–5018. https://doi.org/10.1016/j.jpowsour.2010.02.009

26. Zhang S, Deng C, Fu BL, Yang SY, Ma L (2010) Doping effects of magnesium on the electrochemical performance of Li$_2$FeSiO$_4$ for lithium ion batteries. J Electroanalytical Chemistry 644(2):150–154. https://doi.org/10.1016/j.jelechem.2009.11.035

27. Qu L, Dong L, Shaohua F et al (2016) Mg-doped Li$_2$FeSiO$_4$/C as high-performance cathode material for lithium-ion battery. J Power Sources 307:69–76. https://doi.org/10.1016/j.jpowsour.2015.12.137

28. Zuo P, Wang T, Cheng G, Du C, Ma Y, Cheng X, Yin G (2013) Improved electrochemical performance of nano-crystalline Li$_2$FeSiO$_4$/C cathode material prepared by the optimization of sintering temperature. J Solid State Electrochem 17(7):1955–1959. https://doi.org/10.1007/s10008-013-2042-2

29. Dippel C, Krueger S, Kloepsch R et al (2012) Aging of Li$_2$FeSiO$_4$ cathode material in fluorine containing organic electrolytes for lithium-ion batteries. J Electrochimica Acta 85:66–71. https://doi.org/10.1016/j.electacta.2012.07.109

30. Ou X, Liang G, Wang L, Xu S, Zhao X (2008) Effects of magnesium doping on electronic conductivity and electrochemical properties of LiFePO$_4$ prepared via hydrothermal route. J Power Sources 184(2):543–547. https://doi.org/10.1016/j.jpowsour.2008.02.077

31. Mokhtar A, Ishak MI, Hasanaly SM (2014) Effects of ball milling on the electrochemical performance of Li$_2$FeSiO$_4$ cathode. Adv Mater Res 879:16–20. https://doi.org/10.4028/www.scientific.net/AMR.879.16

32. Liu S, Xu J, Li D, Hu Y, Liu X, Xie K (2013) High capacity Li$_2$MnSiO$_4$/C nanocomposite prepared by sol–gel method for lithium-ion batteries. J Power Sources 232:258–263. https://doi.org/10.1016/j.jpowsour.2012.12.126

33. Zheng Z, Wang Y, Zhang A, Zhang T, Cheng F, Tao Z, Chen J (2012) Porous Li$_2$FeSiO$_4$/C nanocomposite as the cathode material of lithium-ion batteries. J Power Sources 198:229–235. https://doi.org/10.1016/j.jpowsour.2011.09.066

34. Xiang K, Guo H, Li X et al (2008) Influence of synthetic temperature on the electrochemical properties of Li$_2$FeSiO$_4$/C. J Funct Mater 09:1455–1457

35. Boulineau A, Sirisopanaporn C, Dominko R (2010) Polymorphism and structural defects in Li$_2$FeSiO$_4$. Dalton Trans 39:6310–6316. https://doi.org/10.1039/C002815K

36. Yamada A et al (2009) Oral presentation and personal communication, LiBd meeting, Arcachon, France

37. Saracibar A, Van Der Ven A, Arroyo-de Dompablo ME (2012) Crystal structure, energetics, and electrochemistry of Li2FeSiO4 polymorphs from first principles calculations. Chem Mater 24(3):495–503. https://doi.org/10.1021/cm202818u

38. Masquelier C, Croguennec L (2013) Polyanionic (phosphates, silicates, sulfates) frameworks as electrode materials for rechargeable Li (or Na) batteries. Chem Rev 113(8):6552–6591. https://doi.org/10.1021/cr3001862